Archives of Osteoporosis (2019) 14:70
https://doi.org/10.1007/s11657-019-0621-2

ORIGINAL PAPER

Bone measurements at multiple skeletal sites in adolescent idiopathic scoliosis—an in vivo correlation study using DXA, HR-pQCT and QCT

Ka Yee Cheuk[1,2,3] · Yizhong Hu[4] · Elisa M. S. Tam[1,2,3] · Lin Shi[5] · Fiona W. P. Yu[1,2,3] · Vivian W. Y. Hung[1,2,3] · Kevin Cheuk Yin Lai[4] · Wilson Ho Wu Cheng[4] · Benjamin H. K. Yip[6] · Ling Qin[1] · Bobby K. W. Ng[1,2,3] · Winnie C. W. Chu[5] · James Griffith[5] · X. Edward Guo[4] · Jack C. Y. Cheng[1,2,3] · Tsz Ping Lam[1,2,3]

Received: 21 January 2019 / Accepted: 17 June 2019

Abstract

Summary Significant correlations for bone mineral density and bone microstructure between spinal and non-spinal skeletal sites (distal radius and proximal femur) in adolescent idiopathic scoliosis (AIS) patients were observed, indicating that proximal femoral DXA and distal radial HR-pQCT could provide valid clinical assessments in patients with AIS.

Purpose Low bone mass is an important feature of adolescent idiopathic scoliosis (AIS), which is a complex 3D spinal deformity that affects girls during puberty. However, no clinical imaging modality is suitable for regular monitoring on their spinal bone qualities in rapid growth period. Therefore, we investigated whether bone mineral density (BMD) and bone microstructure at non-spinal sites correlated with BMD and mechanical property in the spine in AIS patients.

Methods Thirty-two AIS girls (16.7 ± 3.5 years old with mean Cobb angle of 67 ± 11°) who underwent pre-operative spine CT examination for navigation surgery were recruited. Volumetric BMD (vBMD) of lumbar spine (LS) was measured by quantitative computed tomography (QCT), vBMD and bone microstructure of distal radius (DR) by high-resolution peripheral QCT (HR-pQCT) and areal BMDs of total hip (TH) and femoral necks (FN) by dual-energy X-ray absorptiometry (DXA). Biomechanical properties of the DR and LS were estimated by finite element analysis (FEA). Pearson correlation was performed to study the correlation between bone parameters at these three sites.

Results LS vBMD correlated significantly with both FN and TH aBMD ($R = 0.663$–0.725, both $p < 0.01$) and with DR microstructural parameters ($R = 0.380$–0.576, all $p < 0.05$). Mechanical properties of LS and DR were also correlated ($R = 0.398$, $p = 0.039$).

Conclusions Bone measurement at proximal femur and distal radius could provide an additional predictive power in estimating the bone changes at spine, which is the primary site of deformity in AIS patients. Our result indicated that DXA and HR-pQCT could provide a valid surrogate for spine bone measurements in AIS patients.

Keywords Adolescent idiopathic scoliosis · Bone microstructure · Bone mechanical property · Quantitative computed tomography · Spine · Finite element analysis

Ka Yee Cheuk and Yizhong Hu contributed equally to this work.

✉ Tsz Ping Lam
tplam@cuhk.edu.hk

[1] Bone Quality and Health Centre, Department of Orthopaedics and Traumatology, The Chinese University of Hong Kong, Hong Kong, Hong Kong

[2] SH Ho Scoliosis Research Laboratory, The Chinese University of Hong Kong, Hong Kong, Hong Kong

[3] Joint Scoliosis Research Center of the Chinese University of Hong Kong and Nanjing University, Nanjing, China

[4] Bone Bioengineering Laboratory, Department of Biomedical Engineering, Columbia University, New York, NY, USA

[5] Department of Imaging and Interventional Radiology, Prince of Wales Hospital, The Chinese University of Hong Kong, Hong Kong, Hong Kong

[6] JC School of Public Health and Primary Care, Faculty of Medicine, The Chinese University of Hong Kong, Hong Kong, Hong Kong

Published online: 27 June 2019

Introduction

Adolescent idiopathic scoliosis (AIS) is a complex three-dimensional spinal deformity, which mainly affects girls during the peripubertal period [1, 2]. AIS can be a serious condition with significant morbidity, especially for patients with severe curves. Low bone mineral density (BMD) is an independent and significant prognostic indicator for curve progression, suggesting that abnormal bone metabolism may be an etiologic factor for AIS [2–4]. Assessment of the bone in the spine is therefore important when investigating the etiopathogenesis of AIS. Dual-energy X-ray absorptiometry (DXA) is the current gold standard for areal BMD (aBMD) measurement. However, spine aBMD measurement with DXA is not suitable for patients with scoliosis since aBMD measurement by two-dimensional DXA is not accurate when axial rotation of the spine is greater than 8° [5, 6]. Three-dimensional scanning with quantitative computed tomography (QCT) can provide accurate volumetric BMD (vBMD) measurement of the spine though its routine use in AIS is limited due to radiation concerns.

Given the limited use of QCT of the spine in AIS, previous studies have focused on aBMD, volumetric BMD (vBMD), bone microstructure and bone mechanical property of non-spinal skeletal sites, such as the distal and mid-shaft radius, distal tibia, calcaneus and femoral neck [7–11]. These studies indicated that AIS patients had low BMD and impaired bone qualities compared with age- and sex-matched controls [7–11]. Femoral neck aBMD on the concave side of the major curve measured by DXA [3] and stiffness index of non-dominant calcaneus measured by quantitative ultrasound (QUS) were shown to be significant and independent prognostic factors for curve progression [12]. Cortical vBMD of distal radius measured at the first scoliosis clinical visit was found to improve sensitivity in predicting curve progression [4].

As the prime site of pathoanatomical change in AIS is at the spine, a better understanding of the correlation between bone status of the spine and that of non-spinal skeletal sites should help justify assessment of these non-spinal skeletal sites as valid surrogates for spinal bone measurements. Previous studies on bone loss with aging [13], osteoporotic fracture [14, 15] and rheumatoid arthritis [16] have reported an association in bone density measured at multiple bone sites. These studies involved mainly adults and elderly subjects. Similar studies in young patients diagnosed with AIS are not available in the literature. We hypothesized that BMD and biomechanical property at spine could be estimated by measuring the non-spinal sites for regular monitoring in AIS. This study investigates the correlation between aBMD of femoral neck and total hip measured by DXA, vBMD, bone microstructure and bone mechanical property of distal radius measured by HR-pQCT and vBMD and bone mechanical property of lumbar spine measured by QCT in AIS patients.

Methodology

Subjects, anthropometric, maturity and curve severity measurement

Thirty-two AIS girls at or below 30 years old undergoing corrective spinal surgery were recruited at the Chinese University of Hong Kong. Multidetector CT of the thoracolumbar spine as part of pre-operative preparation for image-guided navigation surgery was performed on all patients. Patients with any disorder affecting bone metabolism, such as genetic disease, chromosomal defect, congenital deformity, neuromuscular disease, autoimmune disorder, endocrine disturbance or previous history of insufficiency fracture, were excluded.

Anthropometric parameters, including body height, body weight, sitting height and arm span, were measured using standard stadiometric techniques [17]. As body height was lost due to spinal deformity, arm span was used to calculate body mass index.

Age of menarche corrected to the nearest month was recorded for each patient. Pubertal maturity was assessed using a self-reported Tanner staging supervised by an experienced technical staff equipped with a Tanner stage pictorial essay [18, 19].

Skeletal maturity was assessed radiologically by an experienced orthopaedic surgeon. Risser sign (range 0–5), reflecting ossification of iliac apophysis on pelvis [20], and recently developed thumb ossification composite index (TOCI) (range 1–8), a simplified staging system based on the ossification pattern of the 2 thumb epiphyses and the adductor sesamoid bone [21], in a hand radiographs were reported. Recent longitudinal study indicated that TOCI could predict the peak height velocity in AIS girls [21], with majority AIS girls attaining their peak height velocity at TOCI stage 5 [21].

Standard standing postero-anterior radiograph of the whole spine was taken prior to surgery for the assessment of curve severity according to the Cobb method [22]. If the subject's spine had more than one curve, Cobb angle of the largest curve was recorded.

QCT measurement of lumbar spine vBMD and FE analysis

Pre-operative CT examination (LightSpeed VCT; GE Healthcare, UK) of the thoracolumbar spine was performed. Machine calibration was performed with the standard phantom before patient scanning. Reconstructed image voxel size was $0.31 \times 0.31 \times 0.63\ mm^3$. To minimize the radiation dose, two slices of QCT images with a 3-sample phantom were scanned at the mid-point of second, third and fourth lumbar (L2, L3 and L4) vertebrae. Vertebra was segmented from the

soft tissue semi-automatically with ITK-SNAP 2.2.0 [23]. Total, cortical and trabecular vBMD (mg/cm^3) of second to fourth lumbar (L2–4) vertebrae were measured by in-house Matlab program from the Department of Imaging and Interventional Radiology at the Chinese University of Hong Kong.

Mechanical properties of the L2–4 vertebra were estimated by finite element (FE) analysis. A schematic for the FE analysis is shown in Fig. 1. The L2–4 vertebrae were extracted by manual segmentation. For each patient, the whole spine CT data was registered to QCT data of the L2, L3 and L4 vertebrae respectively. The CT voxel linear attenuation coefficient values (μ_{CT}) were plotted against the corresponding mineral density values of the QCT data (BMD_{QCT}, obtained from calibration phantom), and the slope and intercepts were used to convert the μ_{CT} values to BMD_{QCT} values. A separate conversion relationship was used for each patient. Each segmented vertebral body was then converted to a FE model using a direct voxel-to-element approach. Vertebral bone tissue was assumed to be anisotropic and elastic [24, 25] with each element assigned heterogeneous tissue properties which is based on previously published density-to-modulus relationship for BMD_{QCT} [26]. Poisson's modulus of bone tissue was assigned as 0.3. In the simulation, a thin layer of PMMA (2.5–5-mm thick, Young's modulus = 2.5 GPa, and Poisson's ratio = 0.3) was added on upper endplate of the vertebra for uniform displacement boundary conditions [24, 25]. The central axis of each vertebra was determined to ensure the applied loading acted along this central axis to mimic vertical load transmission. A uniaxial compression displacement boundary condition was applied to each model [16]. Stiffness as the overall mechanical property of vertebra was determined by FE model with Abaqus 6.7 (SIMULIA, Providence, Rhode Island).

DXA measurement of total hip and femoral neck aBMD

Areal bone mineral density (aBMD; g/cm^2) of bilateral total hip and femoral neck was measured by DXA (Horizon, Hologic, Bedford, MA). Standardized scanning procedure provided by the manufacturer was followed to ensure unified and comparable measurement. Quality assurance was performed by daily calibration against the standard phantoms provided by the manufacturer. The short-term in vivo precision error of aBMD of total hip and femoral neck expressed as coefficient of variation was 2.01 and 0.78% respectively. The spinal aBMD was not measured because this value can be confounded by the rotation the spine in AIS patients, a typical characteristic of scoliosis [6].

HR-pQCT measurement of distal radius vBMD, microstructural and FE analysis

Bone density and microstructure of the non-dominant distal radius were assessed by HR-pQCT (XtremeCT I, Scanco Medical, Brüttisellen, Switzerland). For patients with unfused distal radial growth plates, the scan plane extended 9.02 mm starting 5 mm proximal to a reference line placed at the most proximal aspect limit of the radial growth plate. For patients

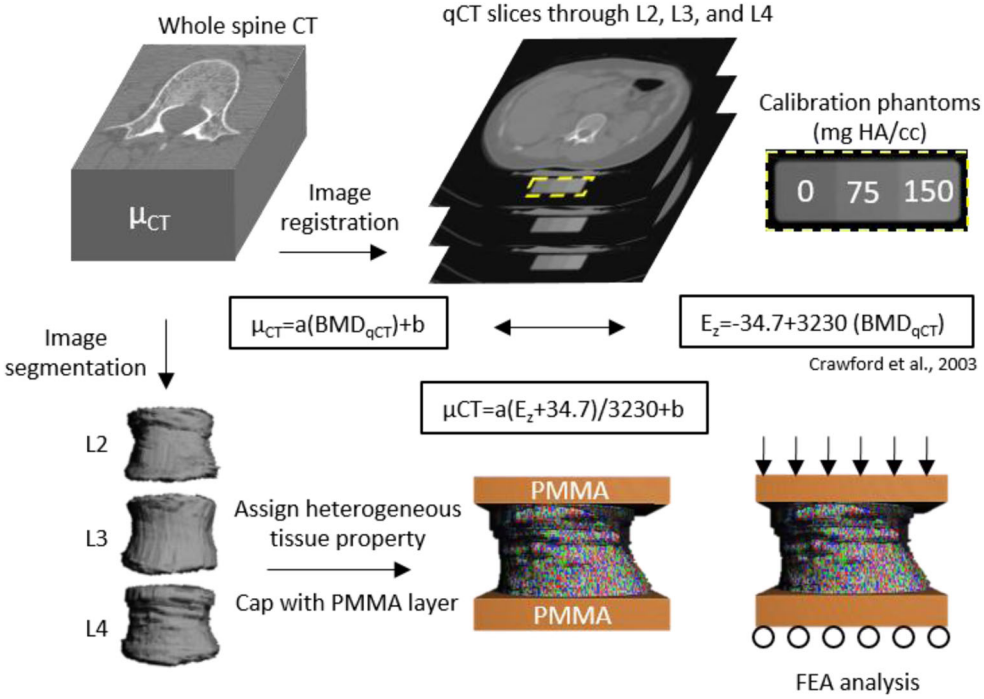

Fig. 1 Schematic for procedures of the FE analysis

with fused distal radial growth plates, the scan plane started 9.5 cm proximal the hump of wrist joint space of the radius [27]. A Gaussian filter was used to remove image noise [28]. An automated threshold-based algorithm was used to separate bone from background soft tissue and cortical bone from trabecular bone [28]. The threshold for the latter was set as one-third of apparent cortical bone density [29]. Total, cortical and trabecular vBMD (mg HA/cm^3) were calculated from the whole bone envelope, cortical bone and trabecular bone respectively.

Total bone area, cortical area and trabecular area (mm^2) were measured directly. Cortical thickness (mm) was calculated as the mean cortical volume divided by the outer cortical surface area [30]. Trabecular bone volume fraction (BV/TV) was derived from trabecular vBMD assuming fully mineralized bone equivalent of 1200 mg hydroxyapatite. Due to partial volume effects, trabecular thickness was calculated by a mid-axis transformation method [31]. Trabecular number (/mm) was defined as the inverse of the mean spacing of trabecular ridges [32]. Trabecular thickness (mm) and trabecular separation (mm) were derived from BV/TV and trabecular number. The short-term in vivo precision errors of densities, areas and microstructural parameters expressed as coefficient of variation were 0.38–1.03%, 0.28–1.86% and 0.80–3.73% respectively.

Stiffness of the distal radius was calculated using FE analysis of HR-pQCT data. A patient-specific micro-FE model of bone was used. The model contained eight-node brick elements of element size $82 \times 82 \times 82$ μm^3. Bone tissue was assumed to be isotropic and linear with a Young's modulus of 10 GPa and a Poisson's ratio of 0.3 [26]. Uniaxial compression testing with 1% strain was performed using manufacturer provided software (μFE Element Analysis Solver v.1.15; Scanco Medical, Switzerland) [26].

Statistical analysis

The required sample size is 31 with the assumption that the correlation coefficient of H1 = 0.55 and H0 = 0, an alpha value of 0.05 and a power of 0.95 (G*Power, version 3.1.9.4, Universitat Kiel, Germany). All bone parameters were tested for normality with Shapiro–Wilk test and all p values were > 0.05. Data were expressed as mean ± standard deviation. Pearson's correlation and scatter plots were used to analyse the correlation between lumbar spine vBMD, mechanical property, and stiffness, femoral neck aBMD and distal radial vBMD, bone microstructure and mechanical property. Hierarchical linear regression analysis was used to determine how femoral neck and distal radius bone parameters explain the variance in total vBMD and mechanical property at the lumbar spine. The limited spatial resolution of lumbar spine QCT data does not permit bone quality measurements, so no correlation between bone microstructure of the lumbar spine and distal radius was performed. All analyses were two-tailed and a p value < 0.05 was considered statistically significant. P values were adjusted by false discovery rate proposed by Benjamini and Hochberg in 1995 [33] to control of multiple comparison effects on the correlations between bone parameters at lumbar spine measured by QCT and those at proximal femur by DXA and at distal radius by HR-pQCT. SPSS (version 25; SPSS Inc., Chicago, IL) was used for statistical analysis.

Results

Demographic data, lumbar spine vBMD and bone mechanical property, total hip and femoral neck aBMD and distal radial vBMD, bone microstructure and mechanical property are shown in Table 1. Patients had a mean age of 16.7 ± 3.5 years old with a mean maximum Cobb angle of 67° ± 11°. All patients attained their peak height velocity (TOCI stage = 7.9), and 91% of them had Risser sign 4/5.

Mean total, cortical and trabecular vBMD of the lumbar spine was 260.7, 376.1 and 187.7 mg/cm^3 respectively. Mean aBMD of the left and right femoral necks were 0.700 and 0.705 g/cm^2 respectively. Mean total, cortical and trabecular vBMD of the distal radius were 311.9, 802.8 and 139.2 mg/cm^3 respectively. The correlations between BMD of lumbar spine, femoral necks and distal radius are shown in Table 2.

Correlation between lumbar spine vBMD and total hip and femoral neck aBMD

aBMDs of both femoral necks and total hip have moderate positive correlation with total and cortical vBMD of the lumbar spine (femoral neck: R ranged 0.603–0.725, total hip: R ranged 0.545–0.711, all $p < 0.01$) (Table 2). Figure 2a is the scatter plot of lumbar spine total vBMD and right femoral neck aBMD.

Correlation between lumbar spine vBMD and distal radius vBMD

The correlation between total, cortical and trabecular vBMD of the distal radius and the lumbar spine was low to moderate ($R = 0.526$, 0.449 and 0.437, $p = 0.004$, 0.016 and 0.019 respectively) (Table 2; Fig. 2d). Figure 2b–d shows the scatter plots of total, cortical and trabecular vBMD between lumbar spine and distal radius.

Correlation between lumbar spine vBMD and distal radial bone microstructure and mechanical property

Correlations between lumbar spine BMD and distal radial bone geometry, trabecular microstructure and bone

Table 1 Physical characteristics and all bone measurements by DXA, HR-pQCT and QCT in surgical AIS patients

	Mean ± SD	Range
Sample size	32	
Physical characteristics		
Age (years)	16.7 ± 3.5	12.8–25.3
Body weight (kg)	46.3 ± 6.3	36.6–60.4
Body height (cm)	156.7 ± 6.7	142.2–170.6
Arm span (cm)	159.0 ± 7.9	146.0–177.0
BMI by arm span (kg/m^2)	18.3 ± 2.4	14.2–22.5
Max Cobb (°)	67.1 ± 10.9	42–87
Maturity		
Menarche age	12.4 ± 0.9	10.1–14.2
Tanner stage (breast)	3.8 ± 1.0	1–5
Tanner stage (pubic hair)	3.6 ± 1.1	2–5
Risser sign	4.2 ± 1.1	0–5
TOCI	7.9 ± 0.5	6–8
Lumbar spine by QCT		
Total vBMD (mg/cm^3)	260.7 ± 33.5	166.2–322.9
Cortical vBMD (mg/cm^3)	376.1 ± 43.5	249.6–457.6
Trabecular vBMD (mg/cm^3)	187.7 ± 31.8	98.7–253.3
Stiffness by FEA (kN/mm)	21.87 ± 5.24	12.72–35.00
Proximal femur by DXA		
Left femoral neck aBMD (g/cm^2)	0.700 ± 0.106	0.527–0.956
Right femoral neck aBMD (g/cm^2)	0.705 ± 0.097	0.550–0.916
Left total hip aBMD (g/cm^2)	0.824 ± 0.021	0.597–1.037
Right total hip aBMD (g/cm^2)	0.819 ± 0.022	0.580–1.039
Distal radius by HR-pQCT		
Total vBMD (mg/cm^3)	311.9 ± 74.7	150.2–498.3
Cortical vBMD (mg/cm^3)	802.8 ± 107.7	577.2–963.4
Trabecular vBMD (mg/cm^3)	139.2 ± 30.3	83.6–219.7
Total area (mm^2)	184.7 ± 33.0	129.7–288.1
Cortical area (mm^2)	41.0 ± 15.2	11.0–63.5
Trabecular area (mm^2)	139.9 ± 32.8	86.0–251.5
Cortical thickness (mm)	0.73 ± 0.27	0.20–1.20
BV/TV	0.116 ± 0.025	0.070–0.183
Tb.N (/mm)	1.541 ± 0.234	1.13–2.02
Tb.Th (mm)	0.075 ± 0.010	0.057–0.105
Tb.Sp (mm)	0.589 ± 0.103	0.422–0.819
Stiffness by FEA (kN/mm)	59.58 ± 13.02	33.65–83.92

aBMD areal bone mineral density, *vBMD* volumetric bone mineral density, *BV/TV* bone volume fraction, *Tb.N* trabecular number, *Tb.Th* trabecular thickness, *Tb.Sp* trabecular separation

Table 2 Pearson's correlation between bone mineral densities (BMD) measured at the lumbar spine, femoral neck, total hip, and distal radius

		Lumbar spine vBMD by QCT	
		Whole bone	Cortical bone
Lumbar spine vBMD by QCT			
Cortical bone	*R*	*0.907***	
	p value	< 0.001	
Trabecular bone	*R*	*0.935***	*0.787***
	p value	< 0.001	< 0.001
Femoral neck aBMD by DXA			
Left	*R*	*0.694***	*0.607**
	p value	< 0.001	0.001
Right	*R*	*0.725***	*0.603**
	p value	< 0.001	0.001
Total hip aBMD by DXA			
Left	*R*	*0.663***	*0.545**
	p value	< 0.001	0.003
Right	*R*	*0.711***	*0.572**
	p value	< 0.001	0.002
Distal radius vBMD by HR-pQCT			
Whole bone	*R*	*0.526**	*0.458**
	p value	0.004	0.015
Cortical bone	*R*	*0.395**	*0.449**
	p value	0.034	0.016
Trabecular bone	*R*	*0.408**	0.156
	p value	0.029	0.429

Significant correlation are italicized

P values were adjusted by Benjamini–Hochberg false discovery rate procedure

aBMD areal bone mineral density, *vBMD* volumetric bone mineral density

mechanical property and stiffness are shown in Tables 3 and 4. Both cortical bone morphometry and trabecular microarchitecture at the distal radius significantly correlated with spinal total vBMD. Cortical and trabecular structures of the distal radius also correlated with spinal cortical and trabecular vBMD respectively. Of the distal radial parameters, cortical area had the highest correlation with spinal cortical vBMD ($R = 0.576$, $p = 0.002$). Significant but low correlation ($R = 0.452$ and 0.470 respectively) was found between distal radial cortical thickness and total and cortical spinal vBMD and between radial trabecular bone volume fraction and trabecular thickness and total and trabecular spinal vBMD (R ranged 0.409–0.515, all $p < 0.05$). Distal radial stiffness correlated moderately (R ranged 0.553–0.652, all $p < 0.01$) with vBMD of the lumbar spine.

Predictive value of femoral neck and distal radial bone parameters for estimating lumbar spine vBMD and stiffness

Table 5 shows the change in R^2 of three-layer hierarchical linear regressions in estimating the total vBMD and stiffness at lumbar spine. Basic patient information, including Cobb angle, age, year since menarche, arm span and body weight, explains 18.5% and 27.7% of the variance in total vBMD and

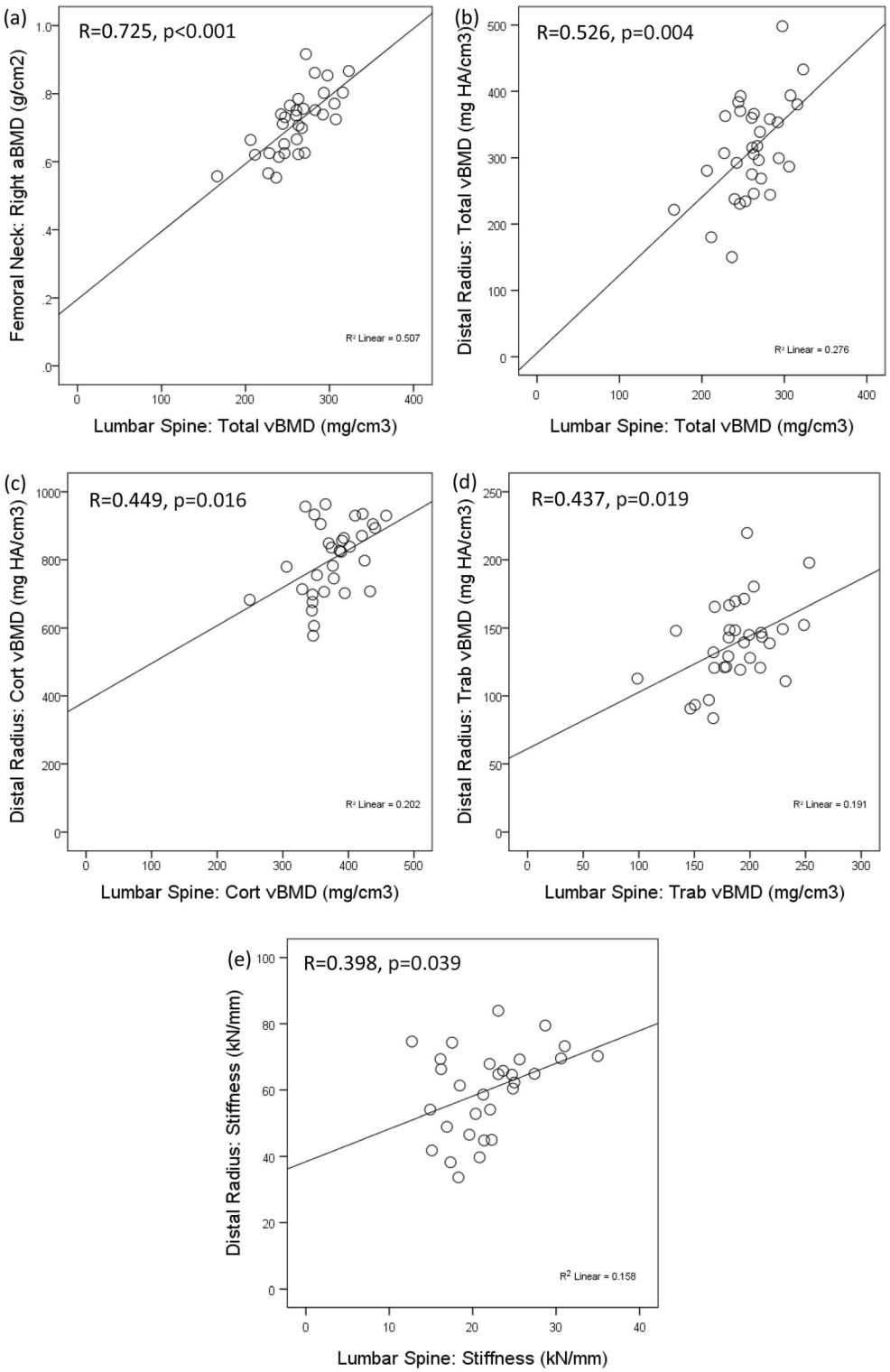

Fig. 2 Scatter plots of bone parameters at lumbar spine, femoral neck, and distal radius. **a** aBMD at right femoral neck by DXA vs. vBMD by QCT at lumbar spine. **b** Total vBMD at distal radius by HR-pQCT vs. that at lumbar spine by QCT. **c** Cortical vBMD at distal radius by HR-pQCT vs. that at lumbar spine by QCT. **d** Trabecular vBMD at distal radius by HR-pQCT vs. that at lumbar spine by QCT. **e** Stiffness at distal radius by HR-pQCT vs. that at lumbar spine by QCT. *P* values were adjusted by Benjamini–Hochberg false discovery rate procedure

stiffness at spine. Femoral neck aBMD explains an additional 43.3% (i.e. 61.8% of total) and 12.9% (i.e. 40.6% of total) of variance. Adding distal radial bone parameters, the model explained 88.1% and 66.7% of the lumbar spine vBMD and stiffness variance respectively.

Discussion

In this study, we investigated the correlation between vBMD and bone mechanical property of the lumbar spine, aBMD of the femoral neck and total hip and vBMD, bone

Table 3 Pearson's correlation between lumbar spine vBMD and distal radius bone geometry and stiffness

Bone geometry Distal radius by HR-pQCT		Lumbar spine vBMD by QCT	
		Whole bone	Cortical bone
Total area	*R*	0.105	0.218
	p value	0.598	0.274
Cortical area	*R*	*0.528**	*0.576**
	p value	0.004	0.002
Trabecular area	*R*	− 0.049	0.036
	p value	0.810	0.843
Cortical thickness	*R*	*0.452**	*0.470**
	p value	0.016	0.013
Stiffness	*R*	*0.652***	*0.638***
	p value	< 0.001	< 0.001

Significant correlation are italicized

microstructure and bone mechanical property of the distal radius in AIS girls. To the best of our knowledge, this is the first study investigating their inter-relationship. Total vBMD of the lumbar spine correlated moderately with both femoral neck and total hip aBMD and low to moderately with distal radial vBMD. Lumbar spine vBMD correlated low to moderately with distal radial bone microstructure, including cortical area, cortical thickness, trabecular bone volume fraction and trabecular thickness and stiffness. These results indicate how BMDs of different skeletal sites correlate with each other in AIS patients. Our result showed that, by hierarchical linear regressions, proximal femoral and distal radial bone parameters explained an additional 69.6% and 39.0% of variance in total vBMD and bone mechanical property at the lumbar spine compared with basic demographic data. The result shows that the derangement in spinal bone density, microstructure and mechanical indices known to occur in AIS patients is systemic in nature.

Table 4 Pearson's correlation between lumbar spine vBMD and distal radius trabecular microstructure and stiffness

Trabecular microstructure Distal radius by HR-pQCT		Lumbar spine vBMD by QCT	
		Whole bone	Trabecular bone
BV/TV	*R*	*0.409**	*0.437**
	p value	0.029	0.019
Tb.N	*R*	0.157	0.192
	p value	0.429	0.337
Tb.Th	*R*	*0.504**	*0.515**
	p value	0.007	0.005
Tb.Sp	*R*	− 0.269	− 0.283
	p value	0.167	0.148
Stiffness	*R*	*0.652***	*0.553**
	p value	< 0.001	0.003

Significant correlation are italicized

P values were adjusted by Benjamini–Hochberg false discovery rate procedure

vBMD volumetric bone mineral density, *BV/TV* bone volume fraction, *Tb.N* trabecular number, *Tb.Th* trabecular thickness, *Tb.Sp* trabecular separation

Compared with the distal radius, aBMD at the femoral neck and total hip had higher correlation with vBMD of the lumbar spine (Table 2). This result is comparable to that of previous studies with significant correlation being found between spine and proximal femur BMD. For example, aBMD of the lumbar spine correlated significantly with that of the proximal femur in both Chinese men and women ($R = 0.84$ and 0.86) [13]. Using QCT, total and trabecular vBMD of L1 was significantly correlated with that of the proximal femur in premenopausal women ($R = 0.68$ and 0.72) [16]. Trabecular vBMD of the lumbar spine by QCT in postmenopausal women showed low ($R = 0.31$) correlation with femoral neck aBMD by DXA [15]. This lower correlation with QCT and DXA comparisons is understandable since QCT and DXA are not measuring the same parameters. Our results show that a greater proportion of variance in the lumbar spine bone parameters can be accounted for after including femoral neck aBMD into the regression model. This positive association between lumbar spine and femoral neck BMD is not surprising since both regions are central weight bearing parts of the skeleton.

vBMD and bone microstructure of the distal radius also positively correlated with that of weight bearing lumbar spine in AIS patients though to a lesser degree than that of the proximal femur as expected (Tables 2, 3 and 4). This is in keeping with the findings of previous studies. All distal radial vBMD by HR-pQCT had low to modest correlation ($R =$ 0.38–0.56) with lumbar spine aBMD by DXA in rheumatoid arthritis patients [14]. Total and trabecular vBMD of the distal radius by HR-pQCT had low to moderate correlation ($R =$ 0.36 and 0.58) with that of L1 measured by cQCT in premenopausal women [16]. The study also reported the correlation between distal radial bone microstructure and L1 vertebral stiffness derived from FEA ($R = 0.38$–0.58) [16]. In postmenopausal women, the BMD correlations were lower ($R =$ 0.18–0.32) [15] when compared to those in our study ($R =$ 0.38–0.65). This suggests that the disparity between the weight bearing spine and non-weight bearing distal radius is greater in postmenopausal women, which might be due to age-dependent differences on the rate of bone loss at different bone sites [34].

It was interesting to note that, among all bone parameters measured by HR-pQCT at distal radius, stiffness derived by FEA has the highest relationship with the lumbar spine vBMD ($R = 0.55$–0.65). Stiffness at distal radius correlated with stiffness at lumbar spine as well ($R = 0.398$, $p = 0.030$) in Fig. 2e.

Table 5 Hierarchical linear regression to determine predictive effect of bone parameters measured at femoral neck by DXA and distal radius by HR-pQCT in estimating total vBMD and stiffness of the lumbar spine by QCT

	R^2	R^2 change	P value of change in R^2
Dependent variable: total vBMD at lumbar spine			
Model 1: basic information	0.185	–	–
Model 2: aBMD at femoral neck	0.618	0.433	<0.001
Model 3: bone parameters at distal radius	0.881	0.264	0.100
Dependent variable: Stiffness at lumbar spine			
Model 1: basic information	0.277	–	–
Model 2: aBMD at femoral neck	0.406	0.129	0.141
Model 3: bone parameters at distal radius	0.667	0.261	0.760

Independent variables in model 1 include Cobb angle, chronological age, year since menarche, arm span and body weight

Independent variables in model 2 include those in model 1 and femoral neck aBMD at both left and right side

Independent variables in model 3 include those in model 2 and all bone parameters measured at distal radius by HR-pQCT, namely, total vBMD, cortical vBMD, trabecular vBMD, total area, cortical area, trabecular area, cortical thickness, trabecular number, trabecular thickness, trabecular separation and stiffness

aBMD areal bone mineral density, *vBMD* volumetric bone mineral density

These results may imply that the stiffness of distal radius derived from FEA based on the HR-pQCT images is a good indicator of the bone mineral status and the overall mechanical index of lumbar spine in AIS patients. Bone parameters at distal radius could provide an additional predictive power in estimating the lumbar spine bone quality when comparing the model with basic information and aBMD at femoral neck as independent variables.

In AIS patients, the main deformity occurs at the spine. DXA measurement is not suitable for the scoliotic spine due to bias from vertebral rotation. Routine QCT is limited by radiation exposure and the general non-availability of body CT systems for QCT examination. This study supports the notion that vBMD and mechanical property of the lumbar spine can be estimated by measuring non-spinal sites such as the femoral neck by DXA and the distal radius by HR-pQCT. This observed relationship helps explain why bone measurements by DXA and HR-pQCT are predictors of disease progression in AIS. Femoral neck aBMD on the concave side was a significant and independent prognostic factor for curve progression in AIS [3]. Significant derangement of cortical compartment (cortical area and thickness) was found in AIS when compared with normal adolescent girls [9]. Baseline Cobb angle $\geq 24°$ and cortical vBMD measured at the distal radius < 570 mg HA/cm^3 are associated with a higher risk of curve progression to the surgical threshold [4]. Based on the results of the current study, DXA measurement of femoral neck and HR-pQCT measurement of distal radius (i.e. vBMD in all compartments, cortical area and thickness, as well as trabecular bone volume fraction and trabecular thickness) were used as valid surrogates for spinal BMD measurement. Bone measurement at appendicular sites, especially the mechanical property and cortical bone parameters (density and size), was shown to reflect spinal bone changes and was used for predicting curve progression.

There are several limitations in this study. Firstly, the patients recruited in this study all had severe AIS curves. Due to ethical reasons, QCT for the spine was not done in the normal growing non-scoliosis adolescent and AIS with mild spinal deformity for comparison. The bone structural and density change during the curve progression phase are not known. Secondly, patients were scanned with two different HR-pQCT scan protocols depending on growth plate fusion. Thirdly, different imaging modalities and segmentation methods were applied in three skeletal sites. It is expected that parameter under the same nature of measurement should yield the highest correlation (e.g. vBMD at spine and vBMD at radius); however, higher correlation between vBMD at spine and aBMD at femoral neck and that between vBMD at spine and stiffness at distal radius were observed in this study. Fourthly, the strategies of FE models in lumbar spine and distal radius were not identical which might introduce variability of stiffness measurement between both sides. Moreover, microstructure and bone mechanical property at the weight-bearing distal tibia were not investigated in this study. The sample size of this study was small. Finally, vBMD measurement of the spine was made at the lumbar rather than the thoracic spine which was the site of main deformity.

In conclusion, we found significant and positive correlations between bone measurements at the lumbar spine, femoral neck, total hip and distal radius. Regular monitoring of BMD and bone mechanical property at spine in AIS patients can be achieved by routine bone assessment on femoral neck by DXA, which involves less radiation when compared with spinal QCT. If HR-pQCT is available, the accuracy can be increased by adding distal radius measurement. These results

will be helpful for investigating bone phenotype and its role in etiopathogenesis of AIS.

Funding information This study was supported by the Research Grants Council of Hong Kong S.A.R., China (Project Nos. 463113 and 14163517) and the National Natural Science Foundation of China (NSFC) and the Research Grants Council (RGC) of Hong Kong Joint Research Scheme (Project No. N_CUHK416/16).

Compliance with ethical standards

Ethical approval All procedures performed in studies involving human participants were in accordance with the ethical standards of the Joint Chinese University of Hong Kong–New Territories East Cluster Clinical Research Ethics Committee (CREC-2013.386) and with the 1964 Helsinki declaration and its later amendments or comparable ethical standards.

Informed consent Written informed consent was obtained from all individual participants and their parents (if patients aged less than 18 years old) before entering the study.

Conflicts of interest None.

References

1. Weinstein SL, Dolan LA, Cheng JC, Danielsson A, Morcuende JA (2008) Adolescent idiopathic scoliosis. Lancet 371(9623):1527–1537
2. Cheng JC, Castelein RM, Chu WC, Danielsson AJ, Dobbs MB, Grivas TB, Gurnett CA, Luk KD, Moreau A, Newton PO, Stokes IA, Weinstein SL, Burwell RG (2015) Adolescent idiopathic scoliosis. Nature Reviews Disease Primers 1:15030
3. Hung VWY, Qin L, Cheung CSK, Lam TP, Ng BKW, Tse YK, Guo X, Lee KM, Cheng JCY (2005) Osteopenia: a new prognostic factor of curve progression in adolescent idiopathic scoliosis. J Bone Joint Surg 87(12):2709–2716
4. Yip BHK, Yu FWP, Wang Z, Hung VWY, Lam TP, Ng BKW, Zhu F, Cheng JCY (2016) Prognostic value of bone mineral density on curve progression: a longitudinal cohort study of 513 girls with adolescent idiopathic scoliosis. Sci Rep 6:39220
5. Larnach TA, Boyd SJ, Smart RC, Butler SP, Rohl PG, Diamond TH (1992) Reproducibility of lateral spine scans using dual energy X-ray absorptiometry. Calcif Tissue Int 51(4):255–258
6. Cheng JCY, Sher HL, Guo X, Hung VWY, Cheung AYK (2001) The effect of vertebral rotation of the lumbar spine on dual energy X-ray absorptiometry measurements: observational study. Hong Kong medical journal = Xianggang yi xue za zhi / Hong Kong Academy of Medicine 7:241–245
7. Lam TP, Hung VWY, Yeung HY, Tse YK, Chu WCW, Ng BKW, Lee KM, Qin L, Cheng JCY (2011) Abnormal bone quality in adolescent idiopathic scoliosis: a case-control study on 635 subjects and 269 normal controls with bone densitometry and quantitative ultrasound. Spine 36(15):1211–1217
8. Cheng JCY, Qin L, Cheung CS, Sher AH, Lee KM, Ng SW, Guo X (2000) Generalized low areal and volumetric bone mineral density in adolescent idiopathic scoliosis. J Bone Miner Res 15(8):1587–1595
9. Yu WS, Chan KY, Yu FWP, Ng BKW, Lee KM, Qin L, Lam TP, Cheng JCY (2014) Bone structural and mechanical indices in Adolescent Idiopathic Scoliosis evaluated by high-resolution peripheral quantitative computed tomography (HR-pQCT). Bone 61:109–115
10. Lee WT, Cheung CS, Tse YK, Guo X, Qin L, Lam TP, Ng BKW, Cheng JCY (2005) Association of osteopenia with curve severity in adolescent idiopathic scoliosis: a study of 919 girls. Osteoporosis Int 16(12):1924–1932
11. Yeung HY, Qin L, Hung VWY, Lee KM, Guo X, Ng BKW, Cheng JCY (2006) Lower degree of mineralization found in cortical bone of adolescent idiopathic scoliosis (AIS). Studies in health technology and informatics 123:599–604
12. Lam TP, Hung VWY, Yeung HY, Chu WCW, Ng BKW, Lee KM, Qin L, Cheng JCY (2013) Quantitative ultrasound for predicting curve progression in adolescent idiopathic scoliosis: a prospective cohort study of 294 cases followed-up beyond skeletal maturity. Ultrasound Med Biol 39(3):381–387
13. Yao WJ, Wu CH, Wang ST, Chang CJ, Chiu NT, Yu CY (2001) Differential changes in regional bone mineral density in healthy Chinese: age-related and sex-dependent. Calcif Tissue Int 68(6):330–336
14. Zhu TY, Griffith JF, Qin L, Hung VWY, Fong TN, Kwok AW, Leung PC, Li EK, Tam LS (2012) Bone density and microarchitecture: relationship between hand, peripheral, and axial skeletal sites assessed by HR-pQCT and DXA in rheumatoid arthritis. Calcif Tissue Int 91(5):343–355
15. Amstrup AK, Jakobsen NF, Moser E, Sikjaer T, Mosekilde L, Rejnmark L (2016) Association between bone indices assessed by DXA, HR-pQCT and QCT scans in post-menopausal women. J Bone Miner Metab 34(6):638–645
16. Liu XS, Cohen A, Shane E, Yin PT, Stein EM, Rogers H, Kokolus SL, McMahon DJ, Lappe JM, Recker RR, Lang T, Guo XE (2010) Bone density, geometry, microstructure, and stiffness: relationships between peripheral and central skeletal sites assessed by DXA, HR-pQCT, and cQCT in premenopausal women. J Bone Miner Res 25(10):2229–2238
17. Cheung CSK, Lee WTK, Tse YK, Tang SP, Lee KM, Guo X, Qin L, Cheng JCY (2003) Abnormal peri-pubertal anthropometric measurements and growth pattern in adolescent idiopathic scoliosis: a study of 598 patients. Spine 28(18):2152–2157
18. Marshall WA, Tanner JM (1969) Variations in pattern of pubertal changes in girls. Arch Dis Child 44(235):291–303
19. Wang Q, Wang XF, Iuliano-Burns S, Ghasem-Zadeh A, Zebaze R, Seeman E (2010) Rapid growth produces transient cortical weakness: a risk factor for metaphyseal fractures during puberty. J Bone Miner Res 25(7):1521–1526
20. Risser JC (1958) The iliac apophysis; an invaluable sign in the management of scoliosis. Clin Orthop 11:111–119
21. Hung ALH, Chau WW, Shi B, Chow SK, Yu FYP, Lam TP, Ng BKW, Qiu Y, Cheng JCY (2017) Thumb ossification composite index (TOCI) for predicting peripubertal skeletal maturity and peak height velocity in idiopathic scoliosis: a validation study of premenarchal girls with adolescent idiopathic scoliosis followed longitudinally until skeletal maturity. J Bone Joint Surg Am 99(17):1438–1446
22. Cobb JR (1960) The problem of the primary curve. J Bone Joint Surg **42-A** 42:1413–1425
23. Yushkevich PA, Piven J, Hazlett HC, Smith RG, Ho S, Gee JC, Gerig G (2006) User-guided 3D active contour segmentation of anatomical structures: significantly improved efficiency and reliability. NeuroImage 31(3):1116–1128
24. Kalender WA (1992) Effective dose values in bone mineral measurements by photon absorptiometry and computed tomography. Osteoporosis Int 2(2):82–87
25. Ma XH, Zhang W, Wang Y, Xue P, Li YK (2015) Comparison of the spine and hip BMD assessments derived from quantitative computed tomography. Int J Endocrinol 2015:675340

26. Crawford RP, Cann CE, Keaveny TM (2003) Finite element models predict in vitro vertebral body compressive strength better than quantitative computed tomography. Bone 33(4):744–750
27. Hung VWY, Zhu TY, Cheung WH, Fong TN, Yu FWP, Hung LK, Leung KS, Cheng JCY, Lam TP, Qin L (2015) Age-related differences in volumetric bone mineral density, microarchitecture, and bone strength of distal radius and tibia in Chinese women: a high-resolution pQCT reference database study. Osteoporosis Int 26(6): 1691–1703
28. Laib A, Ruegsegger P (1999) Calibration of trabecular bone structure measurements of in vivo three-dimensional peripheral quantitative computed tomography with 28-microm-resolution microcomputed tomography. Bone 24(1):35–39
29. Yu WS, Chan KY, Yu FWP, Yeung HY, Ng BKW, Lee KM, Lam TP, Cheng JCY (2013) Abnormal bone quality versus low bone mineral density in adolescent idiopathic scoliosis: a case-control study with in vivo high-resolution peripheral quantitative computed tomography. Spine J 13(11):1493–1499
30. MacNeil JA, Boyd SK (2007) Accuracy of high-resolution peripheral quantitative computed tomography for measurement of bone quality. Med Eng Phys 29(10):1096–1105
31. Laib A, Hildebrand T, Hauselmann HJ, Ruegsegger P (1997) Ridge number density: a new parameter for in vivo bone structure analysis. Bone 21(6):541–546
32. Laib A, Hauselmann HJ, Ruegsegger P (1998) In vivo high resolution 3D-QCT of the human forearm. Technol Health Care 6(5–6): 329–337
33. Benjamini Y, Hochberg Y (1995) Controlling the false discovery rate: a practical and powerful approach to multiple testing. J R Stat Soc Ser B Methodol 57(1):289–300
34. Riggs BL, Melton LJ, Robb RA, Camp JJ, Atkinson EJ, McDaniel L, Amin S, Rouleau PA, Khosla S (2008) A population-based assessment of rates of bone loss at multiple skeletal sites: evidence for substantial trabecular bone loss in young adult women and men. J Bone Miner Res 23(2):205–214